N75-

SEMI-ANNUAL REPORT

For the Period

January 1, 1975 to June 30, 1975

Under NASA Grant NGR 39-009-077

on

Investigation of Critical Burning of Fuel Droplets

by

G. M. Faeth and S. Chanin
Department of Mechanical Engineering
The Pennsylvania State University
University Park, Pennsylvania 16802

July 1975

Semi-Annual Report on the Investigation

of Critical Burning of Fuel Dropelts

Summary

This report discusses activities under NASA Contract NGR 39-009-077 for the period January 1, 1975 to June 30, 1975. During this period, the work was divided into two phases; the results for each phase may be summarized as follows:

1. Oscillatory Combustion of Liquid Monopropellant Droplets. Major emphasis was placed on this portion of the investigation. Analytical efforts were continued for the prediction of open-loop droplet response. The zero-order calculations required in order to predict response were completed for a pressure range of 1-100 atm, over the range of droplet sizes including small droplets which evaporate with little reaction effects and large droplets where the reaction zone is very close to the surface of the droplet. Predictions of gasification rates and liquid surface temperatures were compared to earlier monopropellant droplet combustion measurements in a combustion gas environment. Good agreement was obtained between theory and experiment over the range of the measurements.

   Since the zero-order results were satisfactory, effort has turned to response calculations using the first order analysis. Calculations at the large droplet limit were completed with both quasisteady and unsteady gas models for pressures of 1-100 atm. The open-loop droplet response factor was greater than unity for frequencies extending beyond the characteristic frequency for the liquid phase thermal wave. A second peak is found near the characteristic frequency for gas phase transients, but response in this region cannot be interpreted from simple response factor considerations. Response at the evaporative limit is negative at low frequencies, peaking with a positive value near the liquid phase characteristic frequency. The maximum response factor at this limit is less than unity. Calculations are in progress in the intermediate regime between these limits and these results will be reported later.

   Consideration of droplet response at low frequencies, where the droplet size changes appreciably during a period of oscillation, will be undertaken in the next report period using the zero-order analysis for gasification rate predictions. The related problem of determining spray response from a knowledge of droplet response, at higher frequencies, will also be undertaken at that time.

2. High Pressure Bipropellant Combustion. Work in this area involved extending earlier bipropellant combustion models, valid at low and high pressures respectively, by developing an intermediate pressure model which provides an improved treatment of polar compounds. A second phase of this work involves a generalized analysis of high pressure combustion which allows a simple determination of the conditions required for critical combustion. Difficulties have been encountered with the current intermediate pressure model as its high pressure limit is approached. Work is in progress to resolve this problem.

Table of Contents

List of Figures

List of Tables

Semi-Annual Report for 1975 on the Investigation

of Critical Burning of Fuel Droplets

1. Introduction

The objective of this investigation was to continue earlier work on the steady and unsteady combustion of liquid fuel droplets under rocket engine conditions. Emphasis has been placed on consideration of combustion at elevated pressures and temperatures, representative of typical combustion chamber environments. The results of this study have technical application to the design of liquid fueled rocket engines and the determination of the combustion instability characteristics of these engines.

This report gives a summary of progress on the investigation for the period January 1, 1975, to June 30, 1975. During this report period, the work was divided into two phases, as follows:

1. Combustion response of monopropellant droplets. This portion of the study is concerned with extending the analysis of the "open loop" response of burning monopropellant strands (1,2), to the case of droplets. The basic method employs a perturbation analysis allowing for both liquid and gas phase transient effects. Aside from the overall general problem, several asymptotic regimes can be delineated. This includes evaporation without reaction, a quasisteady gas phase, and the highly reactive regime where droplet curvature effects are negligible. A second category involves the low frequency limit where a single oscillation comprised a large fraction of the lifetime of a droplet and different procedures must be used to compute the response.

2. High Pressure Droplet Burning in Flowing Combustion Gases. The objective of this phase of the investigation is to extend earlier work on bi-propellant droplet combustion (3-6). An intermediate pressure model is under development to provide a continuous transition between present low and high pressure theoretical models; a generalized analysis is also being undertaken in order to obtain guidelines on the characteristics of liquid droplet combustion at elevated pressures; and finally, these results are being integrated in order to determine spray combustion characteristics at supercritical conditions for comparison with experimental results.

During the present report period, major effort was devoted to the area of droplet response and activities in this area will be described in some detail. A brief description of work in the area of high pressure droplet combustion will also be given.

Reports and papers issued during the period of this report are as follows:

G. M. Faeth and S. Chanin, "1974 Annual Report on the Investigation of Critical Burning of Fuel Droplets," Contract NGR 39-009-077, The Pennsylvania State University, University Park, PA, February 1975.

2. Combustion Response of Monopropellant Droplets

2.1 Introduction

The objective of this phase of the investigation involves the determination of the open-loop combustion response of monopropellant droplets to imposed pressure oscillations. Knowledge of the frequency ranges where the combustion response is a maximum, allows the designer either to adjust geometry in order to avoid having characteristic chamber frequencies in this region or provide damping tuned to this frequency range.

The present work is a continuation of earlier efforts on burning liquid monopropellant strands (1,2). In the earlier work, a direct experimental confirmation of the response analysis was obtained. Using these results, the present extension to the case of droplets can be approached with some confidence.

The theoretical approach involves the use of perturbation analysis. The imposed pressure field is decomposed into a constant mean pressure and an oscillatory component having a small amplitude, ε. Decomposing all other quantities in the same manner, solution of the zero order (ε^0) conservation equations give the steady state combustion characteristics. Solution of the first order (ε) conservation equations provide the desired response characteristics; largely manifested by $\dot{m}_1^*$, the amplitude of the gasification rate perturbation (an exception to this occurs in the case of an unsteady gas phase as noted later).

Within the perturbation analysis, several asymptotic regimes may be delineated where substantial simplifications are available for the solution. These regimes are considered separately in the analysis in order to reduce computational effort while still covering a broad range of system variables. Solutions in the asymptotic regimes are also valuable for checking the general analyses which is valid over the entire range.

The asymptotic regimes amy be subdivided with regard to reactivity (droplet size) and frequency, as follows:

1. Reactivity. For a given mean pressure, the distance between the droplet and the zero order reaction zone varies with the size of the droplet. For very large droplets, the reaction zone is close to the droplet and curvature effects are negligible (7), allowing direct use of the earlier strand combustion results (1,2) for the estimation of response (in the following this regime is called the large droplet limit). For very small droplets, the zero order reaction zone is located far from the droplet and fuel simply evaporates and diffuses away from the droplet with little reaction. In this region, the analysis may be simplified by neglecting reaction (small droplet limit). Between these limits there is an intermediate size range where both reaction and curvature are important; here the complete solution must be considered.

2. Frequency. At high frequencies, unsteady effects are important in both gas and liquid phases and the general analysis must be used (an exception occurs at very high frequencies where the liquid no longer responds and only the gas phase is unsteady, but this regime is not considered here). As the frequency of the pressure oscillation is reduced, a region is approached where the gas phase adjusts rapidly to transient effects, while the liquid phase is still unsteady due to its lower thermal diffusi-

vity. In this region, the gas phase is quasisteady, providing a substantial reduction in the complexity of the calculations.

At very low frequencies, the time of an oscillation is no longer small in comparison to the droplet lifetime. In this region the present analysis is no longer valid, and procedures more analogous to vaporization response calculations (8, 9, 10) are more appropriate. This regime will be considered after the calculations for the perturbation analysis are concluded.

2.2 Basic Formulation

A discussion of the assumptions of the analysis; the derivation of the perturbed conservation equations; and the notation of the analysis are all given in Ref. 7. In order to avoid duplication, these results will not be repeated here and the discussion will continue from Section 3.3.4 of Ref. 7.

In the perturbation analysis, any generic dependent variable, G, is assumed to have the form

$$G\ (r,\ t) = G_o\ (r) + \varepsilon\ G_1\ (r)\ e^{i\omega t} \tag{1}$$

where ε represents the small amplitude of the pressure oscillation and all quantities are dimensionless.

Substituting these quantities into the transient conservation equations and separating into like powers of ε gives the zero and first order equations which must be solved.

2.3 Zero-Order Solution

2.3.1 Zero-Order Equations

The zero order, steady state, equations are as follows (7):

$$\dot{m}_{fo} = \dot{m}_o = \text{const.} \tag{2}$$

In the liquid phase, $r < 1$

$$\frac{d}{dr}\ \left(r^2\ \frac{dT_o}{dr} - \frac{\dot{m}_o}{\rho_f \delta_f}\ T_o\right) = 0 \tag{3}$$

In the gas phase, $r > 1$

$$\frac{d}{dr}\ \left(r^2\ T_o\ \frac{d\theta_o}{dr} - \dot{m}_o\ \theta_o\right) = 0 \tag{4}$$

$$\frac{d}{dr}\ \left(r^2\ T_o\ \frac{dT_o}{dr} - \dot{m}_o\ T_o\right) + r^2\ q^{1-n}\ A\ T_o^{\delta-n}\ (\theta_o - T_o)^n\ \exp\ (-E/T_o) = 0 \tag{5}$$

The boundary conditions are:

$$r = 0 \quad , \quad T_o = T_i \tag{6}$$

$$r = 1,$$

$$\lambda_f \left(\frac{dT_o}{dr}\right)_{s-} = T_o \left(\frac{dT_o}{dr}\right)_{s+} - \dot{m}_o \left[(1 - \beta)\, T_o + L\right] \tag{7}$$

$$T_o \left(\frac{d\,(\theta_o - T_o)}{dr}\right)_{s+} = \dot{m}_o \left(\theta_o - T_o - q\right) \tag{8}$$

$$\theta_o - T_o = a\, q \exp\left(- L_f/T_o\right) \tag{9}$$

$$r = \infty \quad , \quad \theta_o = T_o = 1 \tag{10}$$

These equations are sufficiently general to allow for any ambient conditions, either adiabatic or non-adiabatic. Since most combustion chambers are essentially adiabatic, and monopropellants do not involve a local enthalpy defect in any stream (This is only strictly true under the conditions of the present model which allows for temperature gradients in the liquid phase. If there is bulk heating of the liquid small enthalpy defects will arise in the spray.) a condition of adiabatic combustion can be applied. This leads to the zero order compatability condition between dimensionless properties as follows:

$$q = 1 - \beta T_i + L. \tag{11}$$

When Eq. (11) is placed in dimensional form, it provides a computation for the flame temperature.

2.3.2 Zero-Order Liquid Phase

The solution of Eq. (3) can be obtained immediately for the boundary conditions $T_o = T_i$ at $r = 0$ and $T_o = T_{os}$ at $r = 1$, as follows:

$$\frac{T_o - T_i}{T_{os} - T_i} = \exp\left\{\frac{\dot{m}_o}{\rho_f \delta_f}\left(1 - \frac{1}{r}\right)\right\} \tag{12}$$

Evaluating the derivative of Eq. (12) at $r = 1$ and substituting into Eq. (7) yields the boundary condition at $r = 1$,

$$\left(T_o \frac{dT_o}{dr}\right)_{s+} = \dot{m}_o \left(T_o - \beta\, T_i + L\right) \tag{13}$$

2.3.3 General Zero-Order Gas Phase

For the case of adiabatic combustion, integration of Eq. (4) once, application of the boundary conditions at the liquid surface, and the adiabatic flame condition of Eq. (11), yields

$$r^2 T_o \frac{d\theta_o}{dr} - \dot{m}_o \theta_o = - \dot{m}_o \tag{14}$$

Integrating Eq. (14) again, after transformation to eliminate explicit dependence on T_o, yields after application of the outer boundary condition

$$\theta_o = 1 \tag{15}$$

as a consequence of adiabatic combustion. Substituting Eq. (15) into Eq. (8) yields

$$\left(T_o \frac{dT_o}{dr}\right)_{s+} = \dot{m}_o \left(q + T_o - L\right)_s \tag{16}$$

$$T_{os} = 1 - a\, q \exp\left(- L_f / T_{os}\right) \tag{17}$$

which provides a transcendental equation which may be solved for the temperature at the liquid surface. The outer boundary condition, Eq. (10) is unchanged.

The zero order problem is now reduced to the solution of a single, nonlinear, second order, ordinary differential equation, Eq. (5). Equations (10), (16) and (17) provide three boundary conditions to define the problem and determine the eigenvalue, $\dot{m}_o$.

In the general case, Eq. (5) is nonlinear and must be integrated numerically. Since any practical range of numerical integration must be finite with respect to r, the outer boundary condition, Eq. (10), was handled by considering the asymptotic behavior of Eq. (5) for large r.

To find the form of Eq. (5) for large r, let

$$T_o = 1 - \xi T_o^{(1)} \tag{18}$$

where ξ is a small parameter. The radial coordinate is also stretched by defining

$$r = \xi^{\alpha} \eta \tag{19}$$

where α is a constant to be determined by proper matching. Keeping the lowest order terms, the equation becomes:

$$\frac{d}{d\eta}\left(\eta^2 \frac{dT_o^{(1)}}{d\eta}\right) - \dot{m}_o\, \xi^{\alpha} \frac{dT_o^{(1)}}{d\eta} - \xi^{2\alpha + n - 1}\, \eta^2\, A \exp\left(-E\right) T_o^{(1)\, n} = 0 \tag{20}$$

The form of the asymptotic solution depends upon the reaction order, n. The combustion of hydrazine which was considered in Refs. 1 and 2, was best represented by n = 2, which is also generally true for other monopropellants. In this case, a proper match of terms can only be achieved by setting $\alpha = 0$, and balancing convection against diffusion. The resulting asymptotic equation is:

$$\frac{d}{dr}\left(r^2 \frac{dT_o^{(1)}}{dr} - \dot{m}_o T_o^{(1)}\right) = 0 \tag{21}$$

with the outer boundary condition $T_o^{(1)} = 0$, $r = \infty$. Therefore, unlike the strand combustion case (1,2), the asymptotic solution for droplets for n = 2 does not involve the reaction rate term. This occurs since the area for heat conduction increased as r^2 rather than remaining constant, increasing the significance of heat conduction.

The solution of Eq. (21) satisfying the outer boundary condition yields:

$$T_o = 1 - C\,[1 - \exp(-\dot{m}_o/r)] \tag{22}$$

at large r, where the small parameter ξ has been absorbed into the unknown constant, C. The constant C must be determined by matching Eq. (22) with the numerical solution of Eq. (5).

Given A, the solution procedure involves guessing a value for C and $\dot{m}_o$. Starting values for the numerical solution $\left(T_o, \frac{dT_o}{dr}\right)$ are determined from Eq. (22) at some large but finite value of r. Equation (5) is then integrated to the droplet surface, r = 1 using the fourth order Hamming predictor-corrector method. At r = 1, Eqs. (16) and (17) must be satisfied, determining $\dot{m}_o$ and C uniquely. Since Eq. (5) is nonlinear, a double iteration technique must be used. The present procedure employed the Newton-Rapheson method for this iteration. Once $\dot{m}_o$ and C are determined, the outer boundary condition, Eq. (10), is only satisifed at the true mathematical infinity, through Eq. (22).

Initial work on the solution of Eq. (5) involved a "shooting technique" integrating out from the droplet surface and applying the boundary condition of Eq. (10) at a finite value of r. This procedure converged more slowly than the asymptotic method, and gave slightly higher values for $\dot{m}_o$. The "shooting method" became virtually unworkable at large values of A where the reaction zone is very close to the droplet. This experience is generally similar to that encountered during the investigation of strands reported in Refs. 1 and 2.

2.3.4 Gas Phase Solution for Small A.

For a second order reaction, the parameter A in Eq. (5) is proportional to $(p_o^* r_s^*)^2$. Therefore, for small droplet sizes, A approaches zero and the reaction terms may be neglected in the conservation equations. Under these conditions, Eq. (5) may be integrated to yield the following implicit equation for the temperature distribution.

$$\dot{m}_o\left(1 - \frac{1}{r}\right) = T_o - T_{os} + (q - 1)\ln\left\{\frac{T_{os} + q - 1}{T_o + q - 1}\right\} \tag{23}$$

The gasification rate, $\dot{m}_o$, may be determined by applying the outer boundary condition, $T_o = 1$ when $r = \infty$, in Eq. (23) to yield

$$\dot{m}_o = 1 - T_{os} + (q - 1) \ln [1 - (1 - T_{os})/q] \tag{24}$$

The liquid surface temperature, T_{os}, can be determined from Eq. (17).

2.3.5 Zero-Order Gas Phase for Large A

At any pressure, A increases as the size of the droplet increases. With increasing A, the zero-order reaction zone moves closer to the droplet, reducing the influence of curvature on the solution. This is also accompanied by an increase in $\dot{m}_o$, although T_{os} remains unchanged. Reference to the liquid phase solution, Eq. (12), indicates a rapid decay of temperature as one moves into the liquid phase, reducing the effect of curvature in this region as well.

The above discussion indicates that at large A, the process approaches a condition where temperature variation and reaction effects are confined to a thin region surrounding the liquid surface, with little effect of curvature in the spherical coordinate system. Under these conditions, the characteristics of droplet combustion and strand combustion approach one another and the results of Refs. 1 and 2 can be applied directly to the droplet combustion problem. Therefore, it is only necessary to convert the earlier zero-order results to the present notation.

In Refs. 1 and 2, the expression for the liquid surface temperature is equivalent to Eq. (17) and no change is required. Under the present assumptions, particularly unity Lewis number, the curvalinear coordinate system has no influence on the surface temperature. This is also true in cases where the Lewis number is not unity at the high activation energy limit where the reaction zone is collapsed to a flame sheet (11).

In the case of strand combustion, the burning rate eigenvalue is given in terms of a parameter A_s as follows:

$$A_s = \frac{B^* T_{\infty o}^{*\delta} \lambda_{\infty o}^*}{(\rho_{\infty o}^* v_{\infty o}^*)^2 C_p^*} \left(\frac{P_o^*}{M^* R^* T_{\infty o}^*} \right)^n \tag{25}$$

At the large droplet limit, with the combustion zone close to the surface, results

$$\dot{m}_o^* = r_s^{*2} \rho_{\infty o}^* v_{\infty o}^* \tag{26}$$

Therefore, $\dot{m}_o$ is given by

$$\dot{m}_o = (A/A_s)^{1/2} \tag{27}$$

Knowledge of the droplet size and the chemical kinetic parameters provides A;

the quantity A_s is given as the eigenvalue of the zero order solution in Refs. 1 and 2, completing the determination of $\dot{m}_o$.

2.4 Zero-Order Results and Discussion

The physical property values used in the calculations were the same as those used in Refs. 1 and 2 and are representative of hydrazine decomposition. The reaction was taken to be second order, which correlates the bulk of the data in Refs. 1 and 2. The specific value of the various properties and kinetic parameters used in the calculations are summarized in Table 1.

The first check of the zero order model involved comparing predicted and measured liquid surface temperatures as a function of pressure. As noted earlier, the theoretical prediction is independent of geometry under the assumption of unity Lewis number. Therefore, the comparison is identical to that made in Refs. 1 and 2 between measured and predicted surface temperatures in the strand combustion case. These results have been replotted and are shown in Fig. 1. The agreement is good throughout the pressure range of the measurements (.51 - 19.8 atm).

The next set of calculations involved determination of the steady state burning rates and temperature distributions. In addition to the general solution, the large and small A asymptotic cases (large droplet and small droplet limits) were also computed. In order to plot $\dot{m}_o$ as a function of A for the large droplet limit, values of A_s were obtained from the strand combustion calculations. For low activation energies, A_s varies somewhat with pressure. However, for E* given in Table 1 A_s is relatively independent of pressure and the value 1.432×10^7 was used for all conditions (1,2).

Some typical results of the calculations showing $\dot{m}_o$ as a function of A are given in Fig. 2. The conditions for these calculations involved adiabatic combustion at atmospheric pressure with an initial liquid temperature of 298K. The plot shows the small droplet limit (which is independent of A); the large droplet limit (where $\dot{m}_o$ is proportional to A); and the complete solution which provides the transition between these limiting regimes. In this case, the transition region falls in the range $10^4 < A < 10^9$.

Data on hydrazine droplet combustion was available from earlier work done in this laboratory. This involved droplet combustion in a combustion gas, under decomposition conditions for various droplet sizes at atmospheric pressure. The data involved the ambient temperature range 1660 - 2530 K, and it was necessary to extrapolate the values to the 1345 K ambient temperature of the present calculations. The values used in the comparison in Fig. 2 are given in Table 2. The agreement between the predicted and measured burning rate is seen to be quite good, lending confidence to the theoretical model. Notably this correlation was obtained for a value of B^* (in Table 1) which correlates the strand buring rate data at elevated pressures in Refs. 1 and 2. Thus it appears that the droplet measurements at atmospheric pressure are consistent with the second order reaction observed at elevated pressures for strands.

Temperature profiles from the complete solution are shown in Figs. 3 and 4 for the gas and liquid phase. As A increases, the region of substantial temperature gradients is seen to approach the liquid surface. This manifests itself as a reduction in curvature effects and approach to the large droplet limit where adiabatic

Table 1

Properties used in the Theoretical Model

Property	Value
a^* (N/m2)	3.0078×10^{10}
B^* (m^3/Kg-s)	8.385×10^{10}
C_l^* (KJ/Kg-K)	3.0961
C_p^* (KJ/Kg-K)	3.0961
E^* (KJ/Kg-mol)	111700
L^* (KJ/Kg)	1715
L_f^* (KJ/Kg-mol)	40794
Le	1
M (Kg/Kg-mol)	24
n	2
q^* (KJ/Kg)	4937
R^* (KJ/Kg-mol-K)	8.3144
T_i^* (K)	298
$T_{\infty_o}^*$ (K)	1345
γ	1.126
δ	0
λ_l^* (J/m-s-K)	0.390
$\lambda_{\infty_o}^*$ (J/m-s-K)	0.176
ρ_l (Kg/m^3)	1000

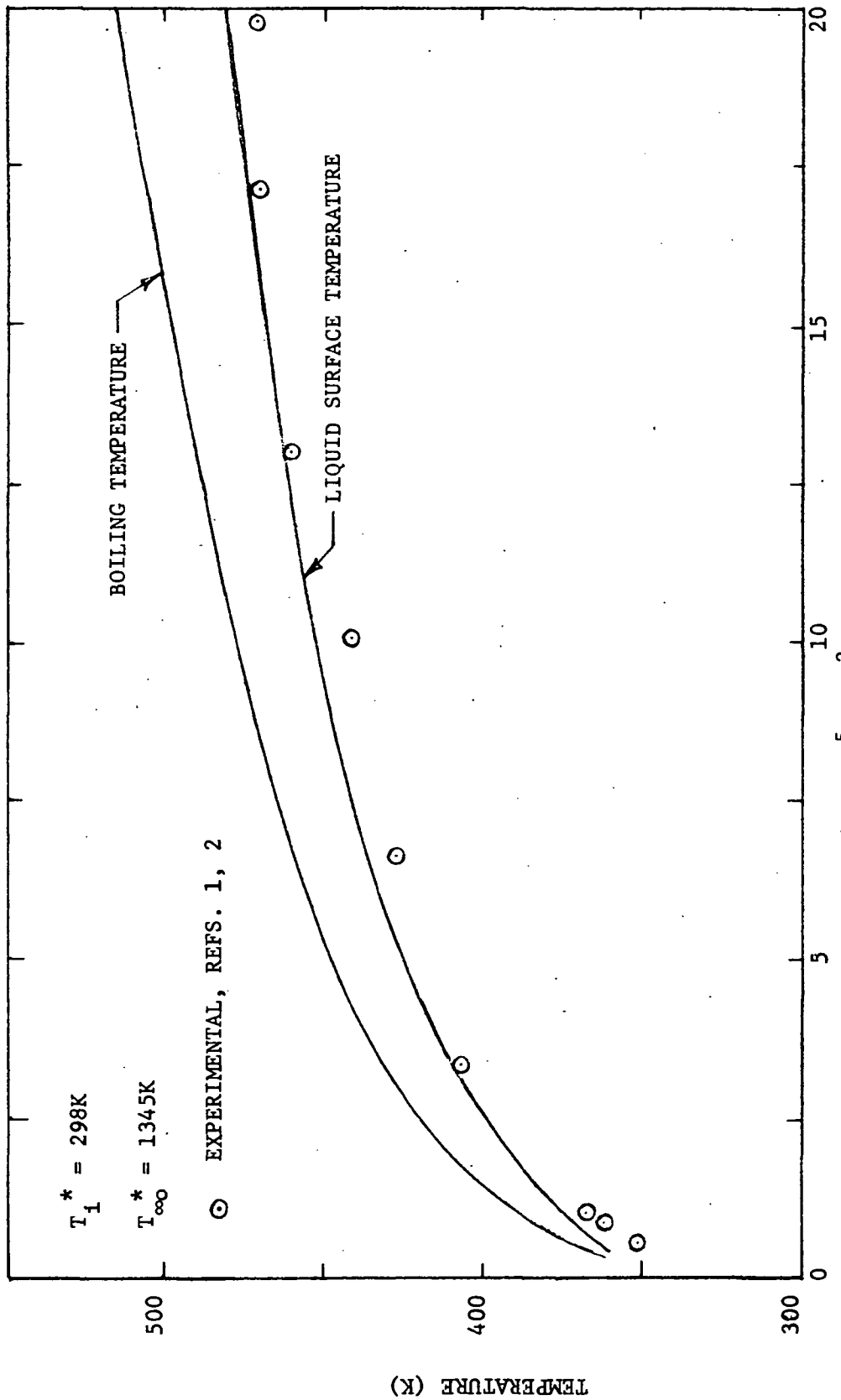

Fig. 1 Theoretical and experimental liquid surface temperature as a function of pressure.

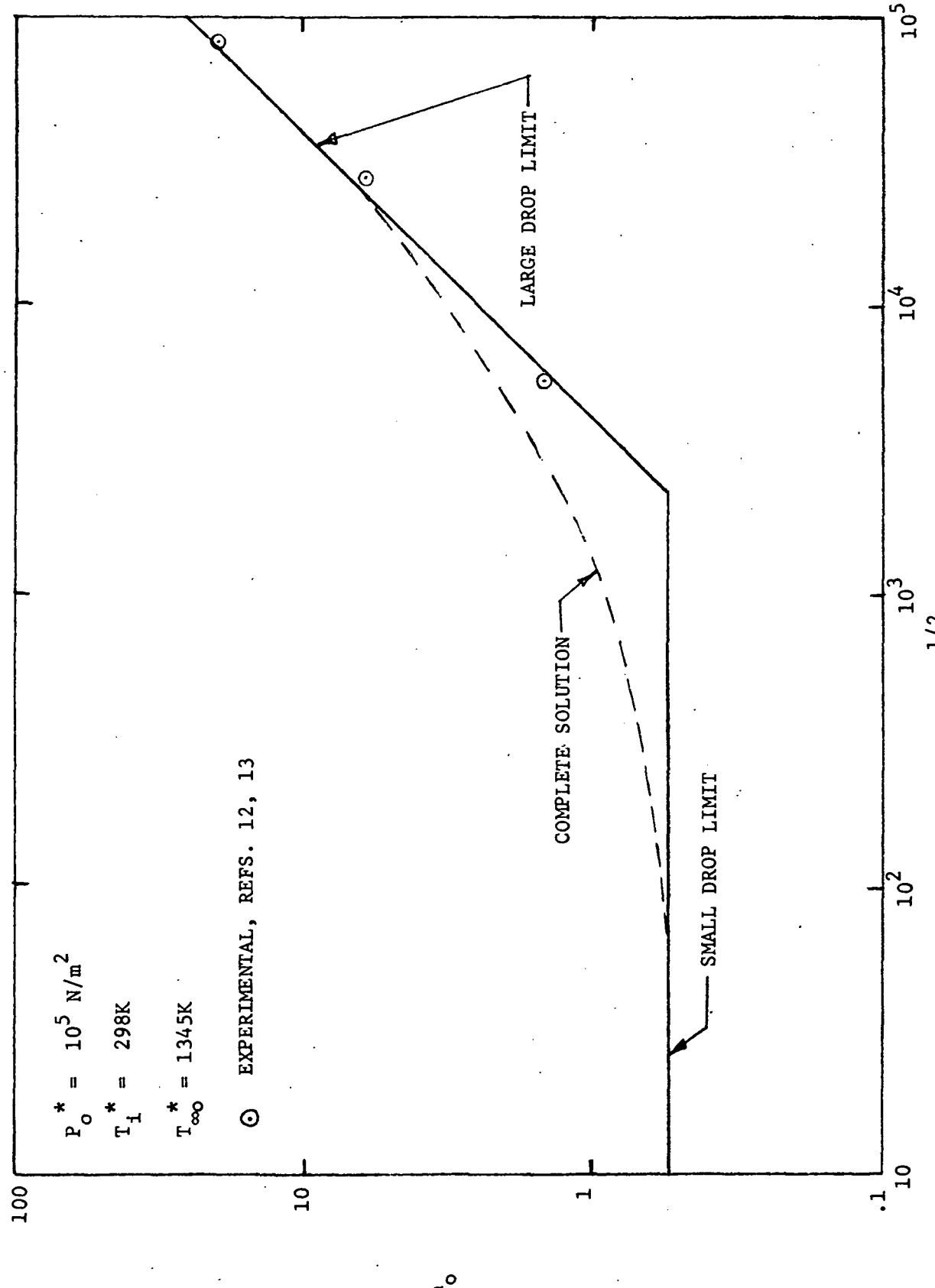

Fig. 2 Theoretical and experimental study steady droplet gasification rates at atmospheric

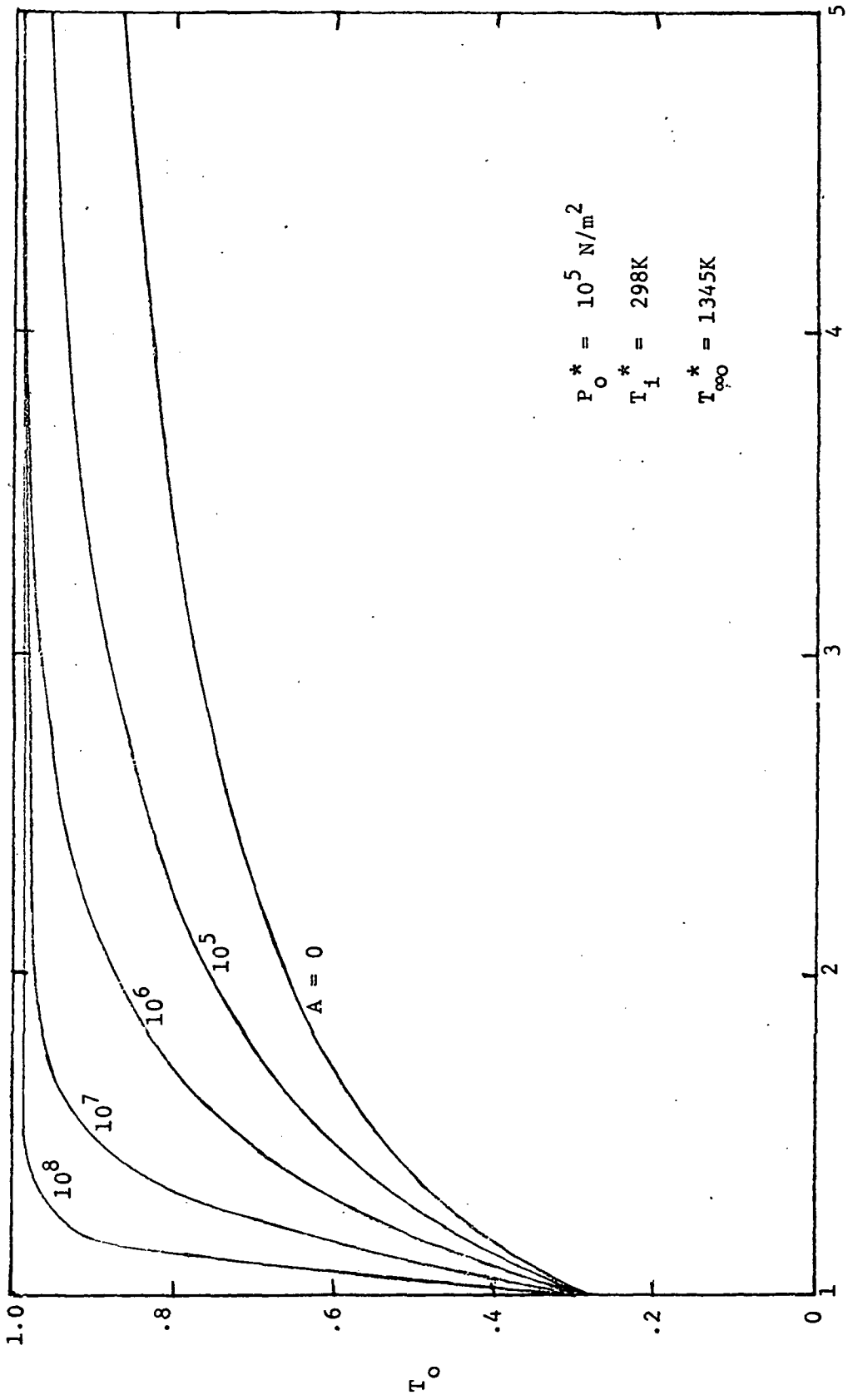

Fig. 3 Steady state gas phase temperatures as a function of A at atmospheric pressure.

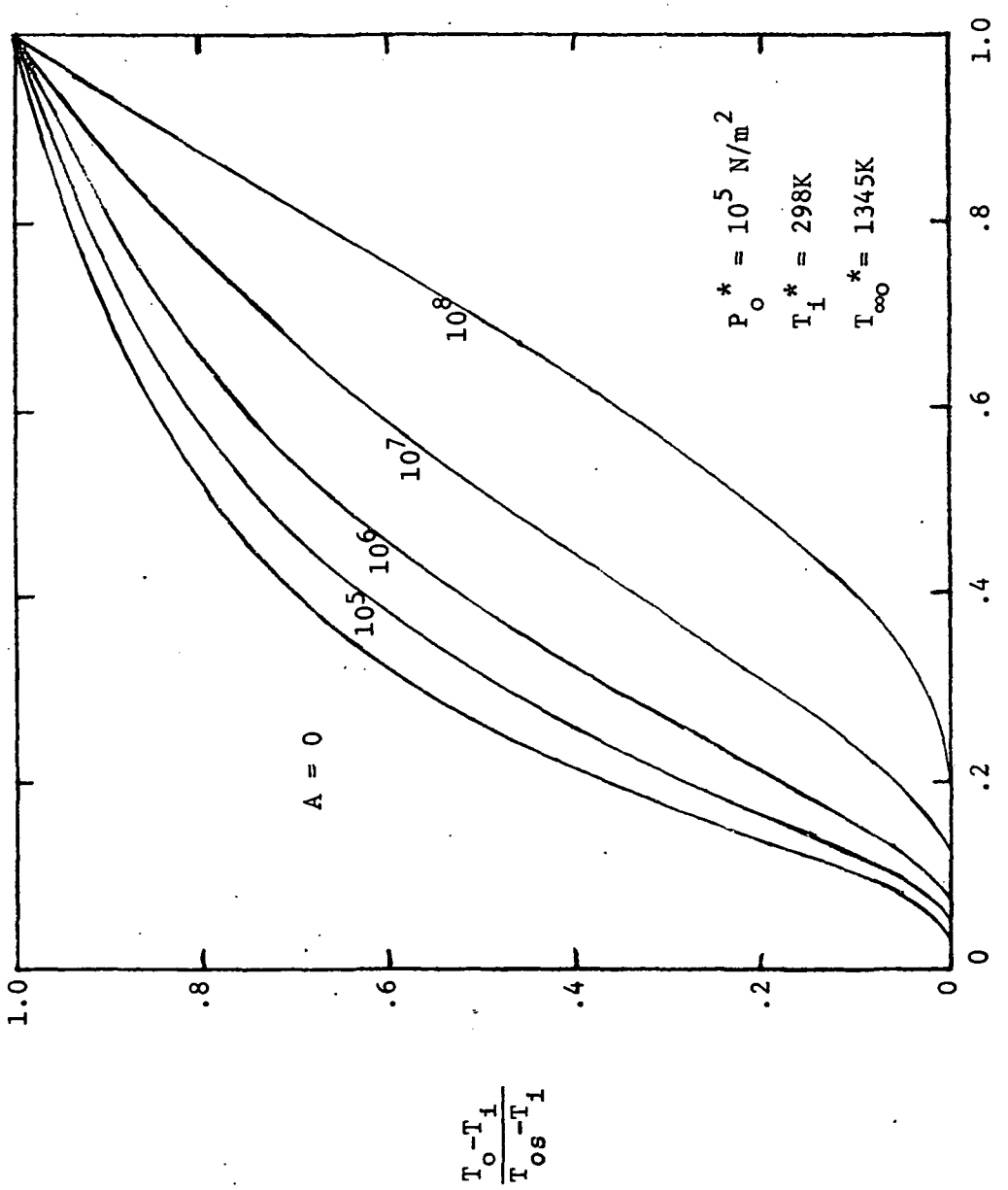

Fig. 4 Steady state liquid phase temperatures as a function of A at atmospheric pressure.

Table 2

Steady Droplet Burning Rate Data[a]

d_s^* (mm)	$4\pi\dot{m}_o^* \times 10^6$ (Kg/s)
1.3	.70
6.3	1.4
19.1	135

[a]Extrapolated to $T_{\infty o}^* = 1345K$ from data of Ref. 12 at atmospheric pressure.

Table 3

Droplet Size Range of Transition Region[a]

$P_o^* \times 10^{-5}$ (N/m^2)	$d_{s_{min}}^* - d_{s_{max}}^*$ (μ)
1	25 - 7500
10	2.5 - 750
100	.25 - 75

[a]Corresponding to $10^4 < A < 10^9$

droplet combustion and strand combustion are essentially the same.

Results at elevated pressures are similar to those at atmospheric pressure, with a range of $10^4 < A < 10^9$ representative of the transition region where both curvature and reaction play a role in the steady droplet combustion reaction. Using properties in Table 1, the droplet size range for this range of A is shown in Table 3. These ranges are somewhat broader than those suggested earlier (Ref. 7) based upon simple flame position arguments. In particular, the small droplet regime is confined to smaller droplets at each pressure. Notably, the size range of technological importance falls largely in the transition region.

2.5 First-Order Solution

2.5.1 First-Order Equations

Utilizing the general zero-order results, the first order equations given in Ref. (7) reduce to the following.

In the liquid phase, $r < 1$

$$\dot{m}_{f1} = \text{const.} \tag{28}$$

$$\frac{d}{dr}\left(r^2 \frac{dT_1}{dr}\right) - \frac{\dot{m}_o}{\rho_f \delta_f} \frac{dT_1}{dr} - \frac{i\omega r^2}{\delta_f} T_1 = \frac{\dot{m}_{f1}}{\rho_f \delta_f} \frac{dT_o}{dr} \tag{29}$$

In the gas phase, $r > 1$

$$T_o^2 \frac{d\dot{m}_1}{dr} - i\omega r^2 T_1 = - i\omega r^2 T_o \tag{30}$$

$$\frac{d}{dr}\left(r^2 T_o \frac{d\theta_1}{dr}\right) - \dot{m}_o \frac{d\theta_1}{dr} - \frac{r^2 i\omega \theta_1}{T_o} = - r^2 \left(\frac{\gamma - 1}{\gamma}\right) i\omega \tag{31}$$

$$\frac{d}{dr}\left(r^2 T_o \frac{dT_1}{dr}\right) - \dot{m}_o \frac{dT_1}{dr} + \frac{d}{dr}\left(r^2 T_1 \frac{dT_o}{dr}\right)$$

$$+ r^2 q w_o \left[(\delta - n) \frac{T_1}{T_o} + n \left(\frac{\theta_1 - T_1}{\theta_o - T_o}\right) + \frac{E T_1}{T_o^2}\right] - \frac{r^2 i\omega T_1}{T_o} =$$

$$\dot{m}_1 \frac{dT_o}{dr} - r^2 \left(\frac{\gamma - 1}{\gamma}\right) i\omega - r^2 q w_o n \tag{32}$$

The boundary conditions are:

$$r = 0 \qquad T_1 = 0 \tag{33}$$

$$r = 1 \qquad \dot{m}_{f1} = \dot{m}_1 \qquad T_{1s} = T_{1s+} \tag{34}$$

$$\lambda_f \left(\frac{dT_1}{dr}\right)_{s-} = T_1 \left(\frac{dT_o}{dr}\right)_{s+} + T_o \left(\frac{dT_1}{dr}\right)_{s+} + \dot{m}_1 \left[(1 - \beta)\, T_o + L\right] - \dot{m}_o (1 - \beta)\, T_1 \tag{35}$$

$$T_o \left(\frac{d(\theta_1 - T_1)}{dr}\right)_{s+} - T_1 \left(\frac{dT_o}{dr}\right)_{s+} = \dot{m}_o (\theta_1 - T_1) + \dot{m}_1 (1 - T_o - q) \tag{36}$$

$$\theta_1 - T_1 = a\, q \exp\left(-L_f/T_o\right) \left[\frac{L_f T_1}{T_o^2} - 1\right] \tag{37}$$

Far from the droplet, θ_1 and T_1 must approach a constant value

$$r = \infty \qquad \theta_1 = T_1 = K_1 \tag{38}$$

The value of K_1 depends upon the case under consideration. For an unsteady gas phase, since $\theta_1 = \theta_1(t)$ at large r, the constant can be determined by considering the behavior of Eq. (31) at large r. In this case, $K_1 = (\gamma - 1/\gamma)$ which is the form for isentropic flow.

In the case of a quasisteady gas phase, with transient effects still important in the liquid phase, K_1 is the amplitude of the ambient temperature variation due to the varying energy content of the liquid at the surface of the droplet (resulting from transient energy storage in the liquid phase.) In this case, K_1 becomes a second eigenvalue in the solution to be determined along with $\dot{m}_1$. At the limit where the liquid phase also becomes quasisteady, the value of K_1 goes to zero, since in the absence of transient energy storage in the liquid phase, Eq. (11) must be satisfied.

The equations for the first order are linear. Therefore, solutions can be combined to eliminate the need for iteration in order to determine $\dot{m}_1$ and K_1. Since the limits of integration extend to infinity, asymptotic gas phase solutions are employed so that numerical computations can be confined to a finite region. Numerical difficulties are encountered in numerically integrating the liquid phase solution to r = 0, therefore an asymptotic analysis is employed in this region as well.

2.5.2 First-Order Liquid Phase

Similar to the zero-order case, the liquid phase solution is completed by applying the boundary condition $T_1 = T_{1s}$ at r = 1, although T_{1s} is not generally known until the gas phase solution is complete. This procedure allows the liquid phase solution to be decoupled from the gas phase.

In order to simplify subsequent discussion, Eq. (29) may be rewritten as:

$$L\{T_1\} = \dot{m}_{f1} H_3 \tag{39}$$

where

$$L = \frac{d^2}{dr^2} + H_1 \frac{d}{dr} + H_2 \tag{40}$$

is a linear operator, and

$$H_1 = \frac{2}{r} - \frac{\dot{m}_o}{\rho_f \delta_f r^2} \tag{41}$$

$$H_2 = - \frac{i\omega}{\delta_f} \tag{42}$$

$$H_3 = (T_{os} - T_i) \frac{\dot{m}_o}{(\rho_f \delta_f r^2)^2} \exp \{\frac{\dot{m}_o}{\rho_f \delta_f} (1 - \frac{1}{r})\} \tag{43}$$

The boundary conditions on Eq. (39) are

$$r = 0, \quad T_1 = 0 \quad ; \quad r = 1, \quad T_1 = T_{1s} \tag{44}$$

The quantity $\dot{m}_1$ is an eigenvalue to be determined from the complete gas and liquid phase solutions. Exploiting the linearity of Eq. (39) let

$$T_1 = \hat{T}_1 + \dot{m}_{f1} T_1^* \tag{45}$$

Equation (45) can be divided into homogeneous and particular parts

$$\hat{T}_1 = \hat{K}_T T_{1H}$$

$$T_1^* = T_{1P}^* + K_T^* T_{1H} \tag{46}$$

where $\hat{K}_T$ and K_T^* are constants to be determined from the boundary conditions. The differential equations then become

$$L \{T_{1H}\} = 0 \quad ; \quad L \{T_{1P}^*\} = H_3 \tag{47}$$

The values of $\hat{K}_T$ and K_T^* are selected to match the boundary condition at r = 1, to yield

$$\hat{K}_T = T_{1s}/T_{1Hs-}$$

$$K_T^* = - T_{1Ps-}^*/T_{1Hs-} \tag{48}$$

In order to match the liquid and gas phase solutions, the derivative of T_l at the liquid surface is required. Combining Eqs. (45), (46) and (48), this quantity is

$$\lambda_f \left(\frac{dT_l}{dr}\right)_{s-} = H_4 T_{ls} + H_5 \dot{m}_{fl} \tag{49}$$

where

$$H_4 = \frac{\lambda_f}{T_{lHs-}} \left(\frac{dT_{lH}}{dr}\right)_{s-} \tag{50}$$

$$H_5 = \lambda_f \left[\left(\frac{dT_{lP}}{dr}\right)_{s-} - \left(\frac{T_{lPs-}^*}{T_{lHs-}}\right) \left(\frac{dT_{lH}}{dr}\right)_{s-}\right] \tag{51}$$

The behavior of Eq. (47) at small r yields the following asymptotic forms for T_{lH} and T_{lP}^* $r \to 0$

$$T_{lH} = \exp\{-\dot{m}_o/\rho_f \delta_f r\} \tag{52}$$

$$T_{lP}^* = \frac{1}{\rho_f \delta_f} (T_{os} - T_i)\left(1 - \frac{1}{r}\right) \exp\left\{\frac{\dot{m}_o}{\rho_f \delta_f}\left(1 - \frac{1}{r}\right)\right\} \tag{53}$$

Equations (52) and (53) formally satisfy the boundary condition $T_l \to 0$, as $r \to 0$. The arbitrary constants in homogeneous equation has been absorbed into $\hat{K}_T$ and K_T^*.

At the limit where $\omega/\delta_f = 0$, the asymptotic forms of Eqs. (52) and (53) are valid throughout the range $0 < r < 1$. At this limit, the solution becomes

$\omega/\delta_f = 0$,

$$T_l = \left[T_{ls} + \frac{\dot{m}_{fl}}{\rho_f \delta_f} (T_{os} - T_i)\left(1 - \frac{1}{r}\right)\right] \exp\left\{\frac{\dot{m}_o}{\rho_f \delta_f}\left(1 - \frac{1}{r}\right)\right\} \tag{54}$$

The solution procedure involves employing Eqs. (52) and (53) to generate starting values for the numerical integration of Eqs. (47), at some small but non-zero value of r. The equations are integrated to the liquid surface, allowing the evaluation of H_4 and H_5 from Eqs. (50) and (51). Substitution of these quantities into Eq. (49) provides the needed expression in the gas phase boundary conditions. Once T_{ls} and $\dot{m}_{fl}$ are determined from the gas phase solution, Eqs. (45), (46) and (47) allow complete determination of T_l in the liquid phase.

2.5.3 First-Order Quasisteady Gas Phase

A number of simplifications are available for the analysis when the gas phase can be assumed to be quasisteady. This limit arises since frequency effects appear as ω in the gas phase and ω/δ_f in the liquid phase. At atmospheric pressure, for hydrazine, δ_f^{-1} has the value 1715 and under these conditions transient effects in the liquid become important at frequencies substantially below the frequencies

where gas phase transients are encountered. Since δ_f is proportional to the mean pressure, the gap between the two characteristic frequencies progressively becomes smaller as the pressure increases.

At the quasisteady gas phase limit, $\dot{m}_1 = \dot{m}_{f1}$, a constant. For adiabatic combustion, consideration of the overall energy balance and integration of Eq. (31) shows that $\theta_1 = K_1$, a constant as well. Equation (32) can then be simplified to yield

$$L' \{T_1\} = A_3 K_1 + A_4 \dot{m}_1 + A_5 \tag{55}$$

where

$$L' = \frac{d^2}{dr^2} + A_1 \frac{d}{dr} + A_2 \tag{56}$$

and

$$A_1 = 2 \left(\frac{1}{T_o} \frac{dT_o}{dr} + \frac{1}{r}\right) - \frac{\dot{m}_o}{r^2 T_o} \tag{57}$$

$$A_2 = \frac{1}{T_o} \frac{d^2T_o}{dr^2} + \frac{2}{r\,T_o} \frac{dT_o}{dr} + \frac{w_o q}{T_o} \left[\frac{(\delta - n)}{T_o} - \frac{n}{(1 - T_o)} + \frac{E}{T_o^2}\right] \tag{58}$$

$$A_3 = \frac{- q\, n\, w_o}{T_o\,(1 - T_o)} \tag{59}$$

$$A_4 = \frac{1}{r^2 T_o} \frac{dT_o}{dr} \tag{60}$$

$$A_5 = \frac{- q\, w_o n}{T_o} \tag{61}$$

The boundary conditions at $r = 1$ become

$$D_1 \left(\frac{dT_1}{dr}\right)_{s+} + D_2\, T_{1s} = D_3\, \dot{m}_1 \tag{62}$$

$$F_1 \left(\frac{dT_1}{dr}\right)_{s+} + F_2\, T_1 = F_3\, K_1 + F_4\, \dot{m}_1 \tag{63}$$

$$G_1 T_1 = K_1 + G_2 \tag{64}$$

where

$$D_1 = T_{os} \tag{65}$$

$$D_2 = \left(\frac{dT_o}{dr}\right)_{s+} - \dot{m}_o\,(1 - \beta) + H_4 \tag{66}$$

$$D_3 = (1 - \beta)\, T_{os} + L + H_5 \tag{67}$$

$$F_1 = - T_{os} \tag{68}$$

$$F_2 = \left(\frac{dT_o}{r}\right)_{s-} + \dot{m}_o \tag{69}$$

$$F_3 = \dot{m}_o \tag{70}$$

$$G_1 = 1 + \frac{a\ q\ L_f}{T_o^{\,2}}\ \exp\ (-\ L_f/T_{os}) \tag{71}$$

$$G_2 = a\ q\ \exp\ (-\ L_f/T_{os}) \tag{72}$$

The outer boundary condition is $r \to \infty$, $T_1 \to K_1$.

Again exploiting linearity, define

$$T_1 = \hat{T}_1 + \dot{m}_1\ T_1^{\,*} + K_1\ \bar{T}_1 \tag{73}$$

Separating the functions in Eq. (73) into homogeneous and particular parts

$$\begin{aligned} \hat{T}_1 &= \hat{T}_{1P} + \hat{K}\ T_{1H} \\ T_1^{\,*} &= T_{1P}^{\,*} + K^*\ T_{1H} \\ \bar{T}_1 &= \bar{T}_{1P} + \bar{K}\ T_{1H} \end{aligned} \tag{74}$$

where

$$\begin{aligned} L'\ \{T_{1H}\} &= 0 & L'\ \{\hat{T}_{1P}\} &= A_5 \\ L'\ \{T_{1P}^{\,*}\} &= A_4 & L'\ \{\bar{T}_{1P}\} &= A_3 \end{aligned} \tag{75}$$

The parameters $\hat{K}$, K^* and $\bar{K}$ are constants which can be selected to satisfy any of the boundary conditions. Since the outer boundary condition can be handled by the asymptotic solution of Eqs. (75), Eq. (64) was chosen to determine the values of the K's. This yields

$$\hat{K} = \left(\frac{G_2}{G_1} - \hat{T}_{1Ps+}\right)/T_{1Hs+} \tag{76}$$

$$K^* = - T_{1Ps+}^{\,*}/T_{1Hs+} \tag{77}$$

$$\bar{K} = \left(\frac{1}{G_1} - \bar{T}_{1Ps+}\right)/T_{1Hs+} \tag{78}$$

The remaining two boundary conditions at r = 1, Eqs. (62) and (63), can be employed to determine the values of $\dot{m}_1$ and K_1. The result is

$$K_1 = (J_{11}\, J_{23} - J_{21}\, J_{13})/(J_{11}\, J_{22} - J_{12}\, J_{21}) \tag{79}$$

$$\dot{m}_1 = (J_{13}\, J_{22} - J_{12}\, J_{23})/(J_{11}\, J_{22} - J_{12}\, J_{21}) \tag{80}$$

where

$$\begin{aligned}
J_{11} &= D_1 \left(\frac{dT_1^*}{dr}\right)_{s+} + D_2\, T_{1s+}^* - D_3 \\
J_{12} &= D_1 \left(\frac{d\bar{T}_1}{dr}\right)_{s+} + D_2\, T_{1s+}^* \\
J_{13} &= -D_1 \left(\frac{d\hat{T}_1}{dr}\right)_{s+} - D_2\, \hat{T}_{1s} \\
J_{21} &= F_1 \left(\frac{dT_1^*}{dr}\right)_{s+} + F_2\, T_{1s}^* - F_4 \\
J_{22} &= F_1 \left(\frac{d\bar{T}_1}{dr}\right)_{s+} + F_2\, \bar{T}_{1s+} - F_3 \\
J_{23} &= F_1 \left(\frac{d\hat{T}_1}{dr}\right)_{s+} - F_2\, \hat{T}_{1s+}
\end{aligned} \tag{81}$$

The derivatives in these expressions are obtained by differentiating Eqs. (74) noting that the K's are constants.

In order to complete the solution, the asymptotic forms of Eqs. (75) at large r must be solved. Proceeding in the same manner as the zero-order case, the result is

$$r \to \infty \qquad T_{1H} = \hat{T}_{1P} = T_{1P}^* = 1 - \exp\,(-\dot{m}_o/r)$$

$$\bar{T}_{1P} = \exp\,(-\dot{m}_o/r) \tag{82}$$

Equations (82) automatically satisfy the outer boundary condition of the gas phase solution.

The solution is obtained by calculating D_1, D_2, D_3, F_1, F_2, F_3, G_1 and G_2 from the zero-order solution and the solution of the first-order liquid phase. The parameters A_1 - A_5 are also available from the zero order solution. Equations (82) are used to generate starting values for the differential equations given by Eqs. (75), at some large but finite value of r. These equations are then integrated to the surface of the droplet. The parameters $\hat{K}$, K^* and $\bar{K}$ can then be

determined from Eqs. (76) - (78). With these parameters in hand, $\hat{T}_{1s}$, T_{1s}^*, $\bar{T}_{1s}$ and the derivatives of these quantities can be determined from Eqs. (74) and the derivatives of these equations. Determining the J_{ij} from Eqs. (81) then allows K_1 and $\dot{m}_1$ to be found from Eqs. (79) and (80). If desired, T_1 can then be evaluated as a function of r from Eq. (73) for the gas phase (yielding T_{1s}) and from Eq. (45) for the liquid phase.

2.5.4 First-Order Unsteady Gas Phase

The methodology for the first-order unsteady gas phase solution is similar to that of the quasisteady gas phase. In this case $\dot{m}_1$ and θ_1 are no longer constants and additional equations must be solved. However, the system of equations is linear so that solutions can be combined to provide a straightforward method without iterations. Asymptotic analysis provides starting conditions for the integration at a large but finite value of r, with integration proceeding to the liquid surface. A full description of this method will be deferred until the end of the next report period.

As noted earlier, the strand results can be used directly at the large droplet limit. In order to consider response, the open-loop droplet response function is employed (8). In the present notation, this quantity is

$$P_r = \text{Re}\ \{\dot{m}_1/\dot{m}_o\} \tag{83}$$

where Re denotes the real part, i.e. that portion of the burning rate oscillation that is in phase with the pressure oscillation. For instability, P_r must be positive and of order unity (the exact value depends upon the degree of damping present) at a point in the combustion chamber when the pressure is varying.

The conversion of r_o and r_1, the strand burning rate and its perturbation, is straightforward at the large droplet limit, namely

$$\text{Re}\ \left\{\frac{\dot{m}_1}{\dot{m}_o}\right\} = \text{Re}\ \{r_1\} \tag{84}$$

since $r_o = 1$. The dimensionless frequency for the strand combustion case, ω_s, is related to the present dimensionless frequency as follows:

$$\omega_s = (A_s/A)\omega \tag{85}$$

As noted earlier, for an activation energy suitable for hydrazine, $A_s = 1.432 \times 10^7$ at mean pressures in the range 1-100 atm. The above transformations are also valid in the quasisteady gas phase limit.

2.6 First-Order Results and Discussion

Calculations are still in progress for the quasisteady and unsteady gas phase response analyses. Therefore, a discussion of the major results will be deferred until the next report period. In order to indicate the scope of the results, however, some initial findings of the analysis will be discussed here. As in the case of the

zero order analysis, properties and kinetic parameters suitable for hydrazine decomposition are employed for the numerical results (Table 1).

Figure 5 illustrates results at the small droplet or evaporative limit, where reaction effects may be ignored. The open-loop droplet response function and the magnitude of the surface temperature oscillation, T_{ls}, are plotted as a function of pressure. The frequency for this plot is zero so that both the gas and liquid phases are quasisteady (The present analysis is not formally valid at $\omega = 0$, since the mean droplet size varies during an oscillation at this condition, therefore, the plot should be taken as representative of conditions where it is still valid to assume that both gas and liquid phases are quasisteady but with sufficiently high frequency so that changes in mean size can be ignored during a period of oscillation).

At this condition, the open-loop response function is negative, with a relatively small magnitude. This is in contrast to results for bipropellant combustion where the response function generally approaches zero or a positive limit for small ω. With increasing pressure, the open loop response function becomes more negative.

The surface temperature oscillation is in phase with the pressure oscillation, and its magnitude increases as the pressure increases. This behavior results primarily from the form of the vapor pressure curve. At the quasisteady limit

$$T_{ls} \approx \frac{T_{os}^2}{L_f}$$

therefore since T_{os} increases with increasing mean pressure, T_{ls} increases accordingly.

At the same limit, using the result for T_{ls}

$$\dot{m}_l \approx \frac{-T_{os}^3}{L_f\,[q + T_{os} - 1]}$$

This approximate formula indicates negative response at the quasisteady limit. With increasing pressure, T_{os} increases, providing a larger negative response.

Physically, the negative response at the totally quasisteady limit is caused by the fact that the gasification rate decreases at the surface temperature increases for a constant ambient temperature. At the quasisteady limit, the ambient temperature (corresponding to the adiabatic flame temperature) is independent of temperature-satisfying this condition. During the rising portion of a pressure oscillation, the surface temperature increases in step to keep the mass fraction at the liquid surface approximately constant. This causes reduced rates of gasification at pressures above the mean and increased rates at pressures below the mean--providing a negative response.

As the frequency is increased, within the quasisteady gas phase limit, the ambient temperature also begins to oscillate with finite magnitude. This is due to the thermal wave in the liquid phase varying the total energy content of the flow as it reaches the liquid surface. This effect compensates for the higher liquid temperatures at pressures above the mean, tending to make the response positive. A second factor arises near the characteristic frequency of the liquid phase thermal wave. As the surface temperature begins to lag the pressure oscillation, the liquid temperature gradient at the surface becomes negative and supplements the energy flow

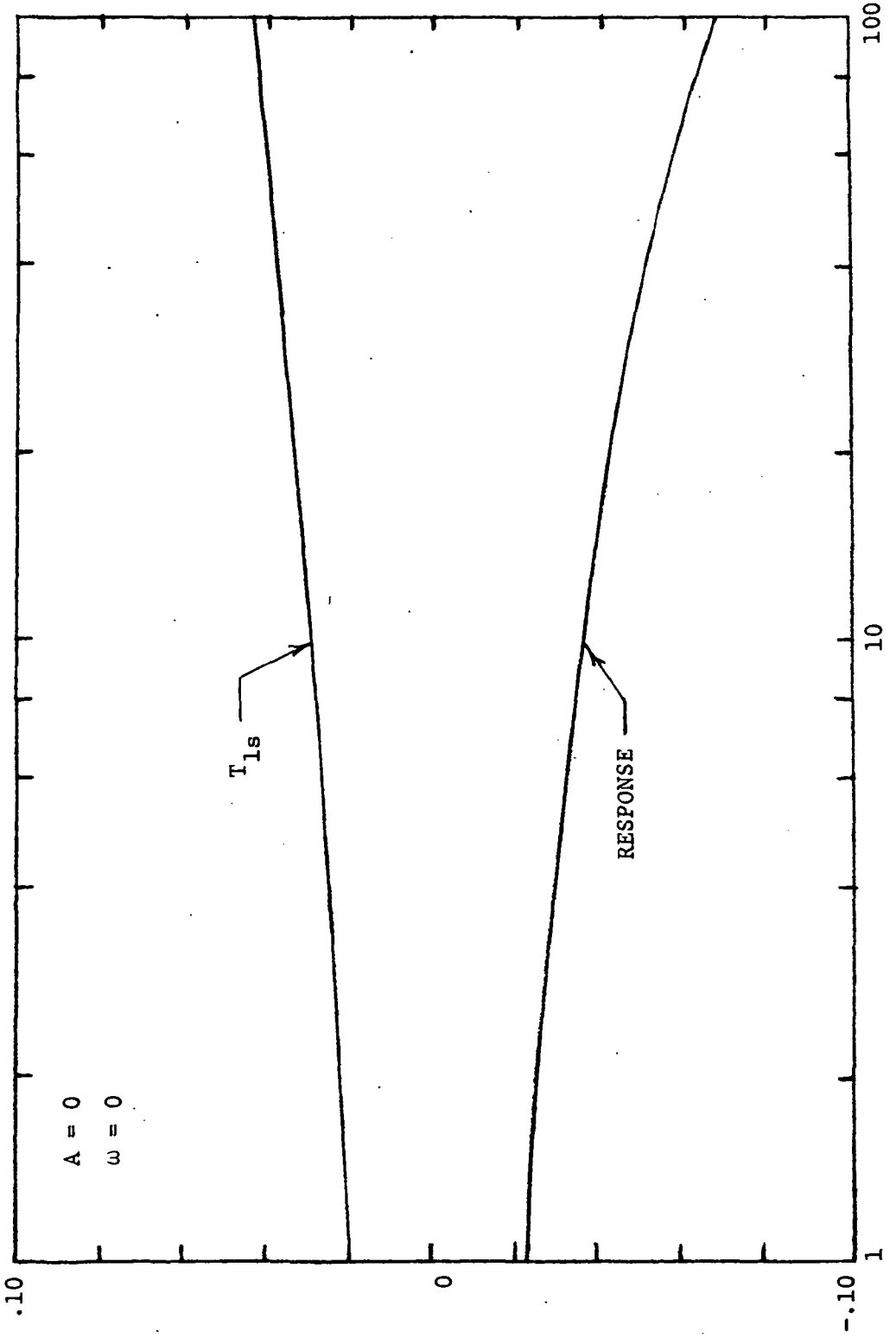

Fig. 5 Open-loop droplet response and surface temperature perturbation as a function of pressure at the small droplet limit.

to the surface--increasing the gasification rate at pressures above the mean. This leads to a peaking of the response at this frequency level, but while the response is positive it is not very large (order 0.5). These results will be documented more fully in the next report. Based on present findings it appears that droplets at the evaporative limit do not contribute substantially to the response of the combustion process, due to their relatively low response.

Moving from the evaporative limit to the other end of the scale, the large droplet limit, much greater response is observed for monopropellant droplets. Figures 6, 7 and 8 illustrate the open-loop droplet response as a function of frequency for large droplets at mean pressures of 1, 10 and 100 atm. In addition to the quasisteady gas phase results, findings allowing for a completely unsteady gas phase are also shown.

At the large droplet limit, the response is essentially unity at low frequencies for a second order reaction. With increasing frequency a peak is reached at frequencies near the characteristic frequency of the liquid phase. This arises largely due to an increase of flame temperature when the pressure is above the mean, resulting from optimum energy storage in the liquid phase. As might be expected, the magnitude of this peak depends upon the activation energy of the reaction, increasing with increasing activation energy. Beyond the peak, the quasisteady gas phase solution gives a continuously declining response, similar to the case of the evaporative limit. At higher frequencies, transient gas phase phenomena become important, leading to a second peak in the open-loop droplet response function.

Comparing Figs. 6, 7 and 8, it is evident that the magnitude of the first response peak increases with increasing pressure. Therefore, large droplets at high pressures contribute most to the response, while small droplets contribute very little at all pressures. Response calculations in progress in the intermediate regime will complete information on the transition between these two limiting cases.

2.7 Low-Frequency Limit and System Analysis

As noted earlier, the previous response analysis is not valid at very low frequencies where the size of a droplet varies appreciably during a period of pressure oscillation. In order to obtain response in this region lifetime calculations must be undertaken, similar to those of Refs. 9 and 10, under conditions where an oscillatory pressure variation is imposed upon the combustion process.

Evaluation of the response of a spray at higher frequencies involves a weighted combination of the response of all droplet sizes present in the combustion field. This calculation also requires computation of droplet life histories in order to determine the size distribution within the spray.

Work on the formulation and analysis of these two related problems will begin in the next report period. The zero-order analysis for droplet response will be employed to estimate the gasification rate of the droplets. This will not require any recalculation of zero-order results, since the existing findings (for example Fig. 2) can be correlated rather simply in terms of droplet size at any given pressure.

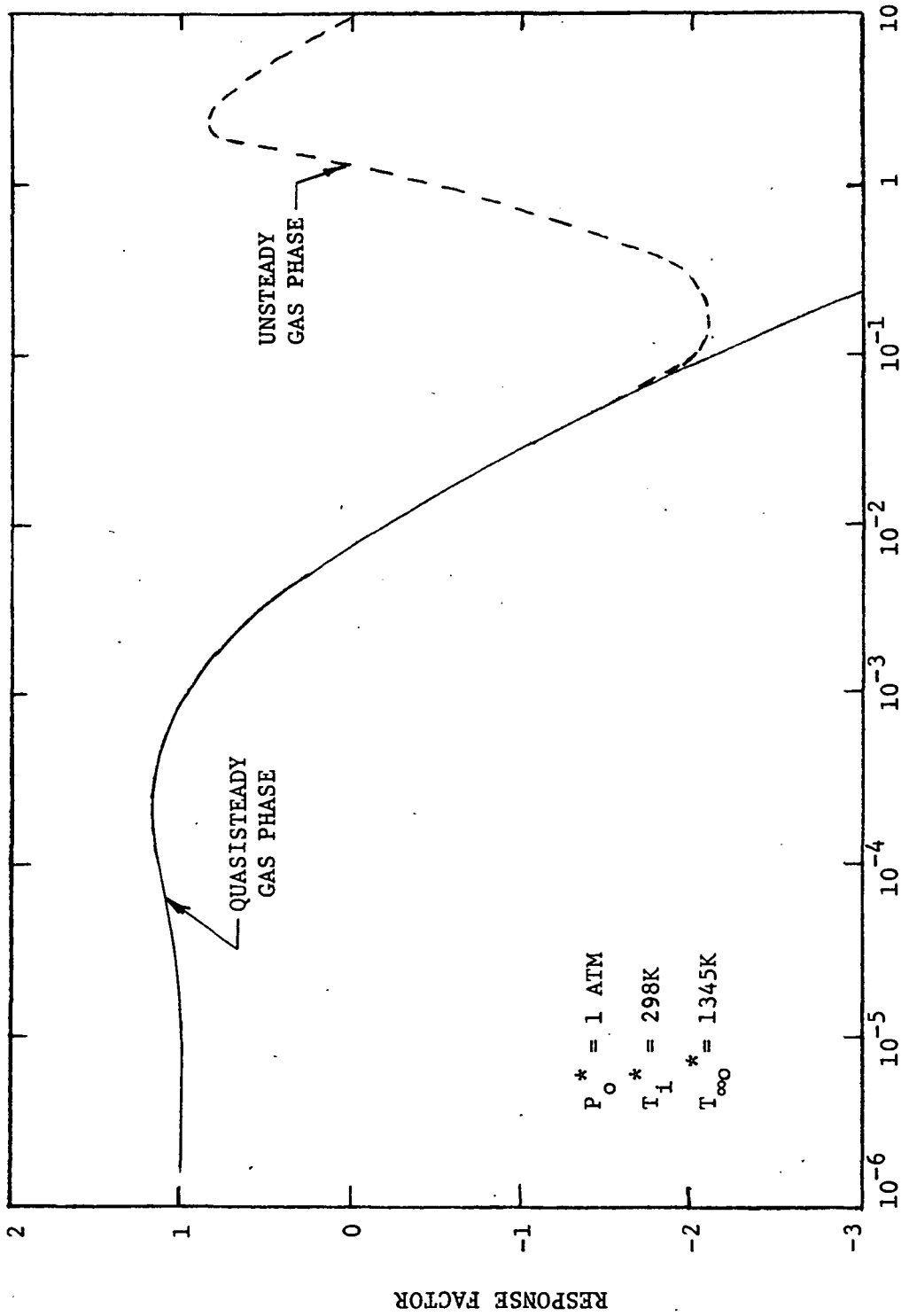

Fig. 6 Open-loop droplet response as a function of frequency at the large droplet limit and a pressure of 1 atm.

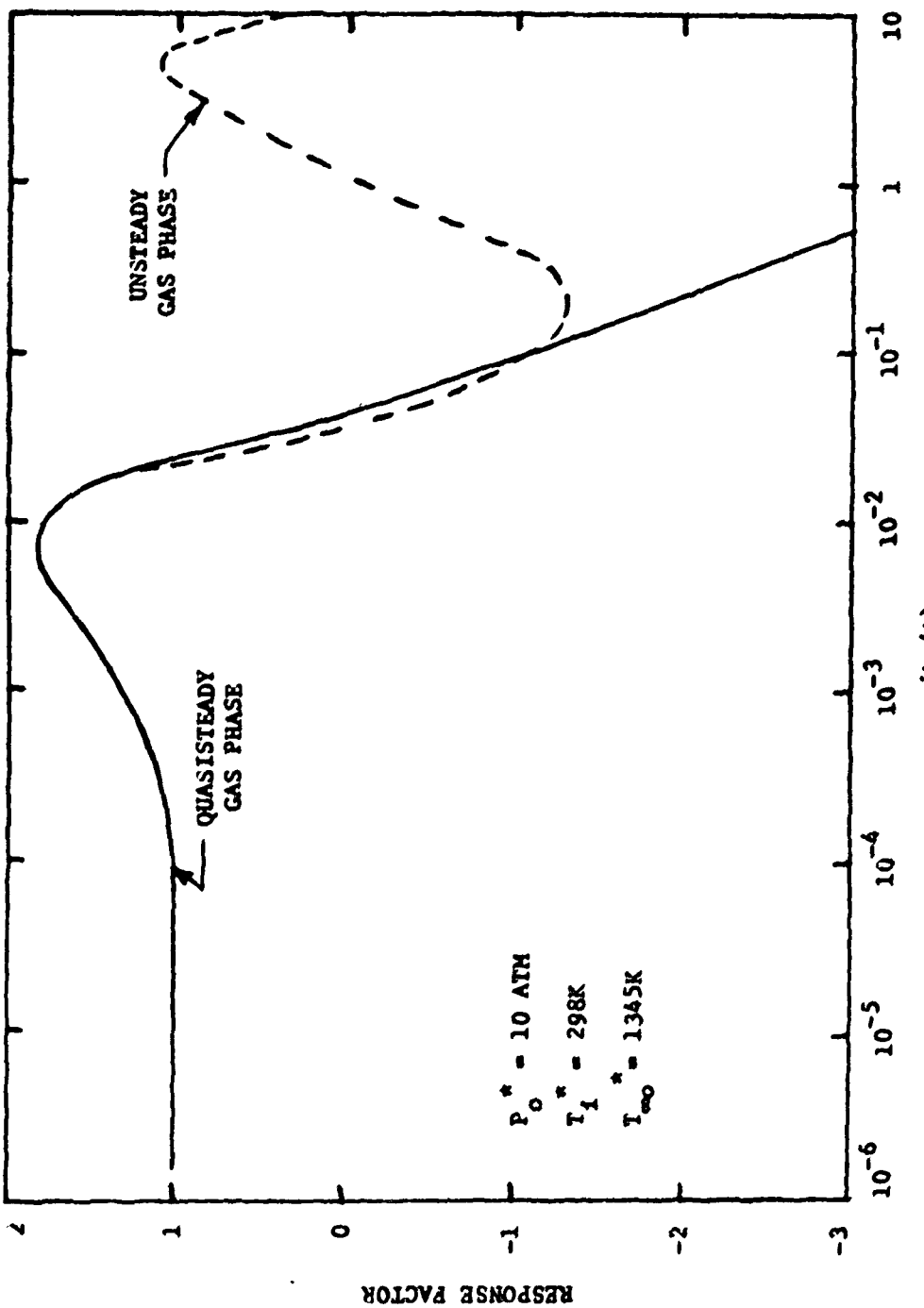

Fig. 7 Open-loop droplet response as a function of frequency at the large droplet limit and a pressure of 10 atm.

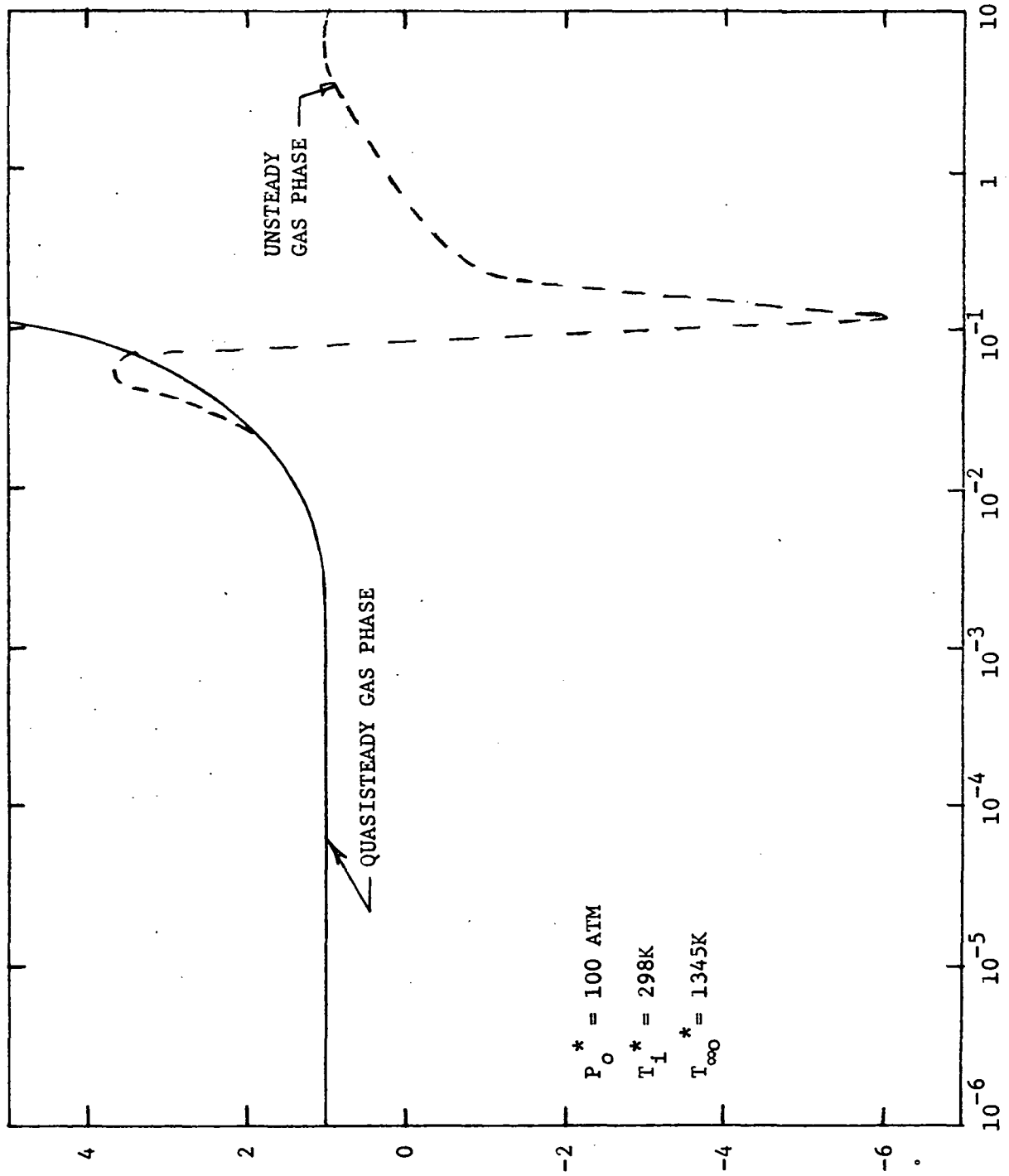

Fig. 8 Open-loop droplet response as a function of frequency at the large droplet limit and a pressure of 100 atm.

2.8 Summary

An analysis has been developed to compute the combustion response of monopropellant droplets (the open-loop droplet combustion response). Under conditions where the droplet size does not change appreciably during a period of oscillation, the method is developed as a perturbation analysis withthe response given by the first-order solution. Asymptotic analysis is employed to treat boundary conditions at infinity and zero.

Calculations were completed for the zero-order steady state at pressures of 1-100 atm, and droplet sizes extending from the evaporative limit(where reaction effects are small) to the highly reactive limit where the combustion zone is close to the droplet. The temperature and burning rate predictions of this analysis were compared with earlier measurements of droplet combustion in an environment typical of an actual combustion chamber. The agreement between theory and experiment was excellent, indicating that the model gives a good representation of the combustion process. This provides some encouragement to continue with the response analysis.

Response calculations are in progress. Work at the large droplet limit is complete for both a quasisteady and unsteady gas phase. Work at the evaporative limit and in the transition region for a quasisteady gas phase is nearing completion. Results for an unsteady gas phase under these conditions will be completed in the next report period.

Analysis of the low frequency limit where the droplet size varies appreciably during a pressure oscillation, and the combination of individual droplet response to obtain the response of a spray are related problems. These calculations involve application of computations that are currently in progress and will be undertaken in the next report period.

3. High Pressure Bipropellant Combustion

3.1 Introduction

Earlier work on the comparison between predicted and measured droplet temperatures and gasification rates at elevated pressures in flowing combustion gases has been concluded. Results indicated satisfactory modeling at low pressures using a conventional model, and satisfactory modeling near the critical point using a high pressure phase equilibria model.

Current effort involves development of an intermediate pressure model to provide a continuous transition between these two limiting cases. A second area of effort involved generalizing the results in order to provide a simple correlation for the evaluation of high pressure effects for given combustion chamber conditions.

3.2 Intermediate Pressure Model

The intermediate pressure model has been coded for the computer, but problems have been encountered in debugging the routine. In particular, difficulties have arisen in obtaining proper asymptotic behavior toward the high pressure limit.

Work is in progress to resolve these difficulties and results should be in

hand at the end of the next report period.

Wilson parameters and Henry's constants have been accumulated for the paraffinic hydrocarbons and some of the air gases (N_2, O_2, H_2O, CO_2). The literature will continue to be surveyed in order to expand the data base of the analysis.

3.3. Generalized Analysis

Work with the generalized analysis has been deferred until the difficulties with the intermediate pressure analysis are resolved.

3.4 Summary

The intermediate pressure model has been coded, but problems were encountered in obtaining the proper asymptotic behavior at elevated pressures. Work is in progress to resolve these difficulties and results should be available at the end of the next report period.

References

1. C. B. Allison, "Burning Rate Response of Liquid Monopropellants to Imposed Pressure Oscillations," NASA CR-134541, January, 1974; also Ph.D. thesis, The Pennsylvania State University, University Park, PA, March, 1974.

2. C. B. Allison and G. M. Faeth, "Open-Loop Response of A Burning Liquid Monopropellant," to be published, AIAA J.

3. G. S. Canada, "High Pressure Combustion of Liquid Fuels," NASA CR-134540, January, 1974; also Ph.D. Thesis, The Pennsylvania State University, University Park, PA, March, 1974.

4. G. S. Canada and G. M. Faeth, "Combustion of Liquid Fuels in a Flowing Combustion Gas Environment," Fifteenth Symposium (International) on Combustion, The Combustion Institute, Pittsburgh, Pennsylvania, (in press).

5. G. S. Canada and G. M. Faeth, "Fuel Droplet Burning Rates at High Pressures," Fourteenth Symposium (International) on Combustion, The Combustion Institute, Pittsburgh, Pennsylvania, pp. 1345-1354, 1973.

6. R. S. Lazar and G. M. Faeth, "Bipropellant Droplet Combustion in the Vicinity of the Critical Point," Thirteenth Symposium (International) on Combustion, The Combustion Institute, Pittsburgh, Pennsylvania, pp. 743-753, 1971.

7. G. M. Faeth and S. Chanin, "1974 Annual Report on Investigation of Critical Burning of Fuel Droplets," NASA CR-134793, February, 1975.

8. Harrje, D. T. (Ed.), Liquid Propellant Rocket Combustion Instability, NASA SP-194, National Aeronautics and Space Administration, Washington, D.C., pp. 128-138, 1972.

9. M. F. Heidmann and P. R. Wieber, "Analysis of Frequency Response Characteristics of Propellant Vaporization," AIAA Paper No. 66-604, 1966.

10. V. D. Agosta and S. S. Hammer, "Vaporization Response of Evaporating Drops with Finite Thermal Conductivity, NASA CR-2510, 1975.

11. G. M. Faeth, "High Pressure Liquid Monopropellant Strand Combustion," Combustion and Flame, Vol. 18, No. 1, pp. 103-113, February 1972.

12. C. B. Allison and G. M. Faeth, "Decomposition and Hybrid Combustion of Hydrazine, MMH and UDMH as Droplets in a Combustion Gas Environment," Combustion and Flame, Vol. 19, No. 2, pp. 213-226, 1972.

13. C. B. Allison, "Hybrid and Decomposition Combustion of the Hydrazine Fuels," NASA CR-72977, July 1971.

Distribution List

NASA
Scientific and Technical Information
Facility - Acquisitions Branch
P.O. Box 8757
Baltimore/Washington International Airport
Baltimore, MD 21240

R. Weiss
AFRPL
Edwards, CA 93523

Dr. R. J. Priem MS 500-209
NASA, Lewis Research Center
21000 Brookpark Road
Cleveland, OH 44135 (2)

University of Wisconsin
Mechanical Engineering Dept.
ATTN: P. S. Myers
1513 University Avenue
Madison, Wisconsin 53705

T. Inouye, Code 4581
U.S. Naval Weapons Center
China Lake, CA 93555

NASA
George C. Marshall
Space Flight Center
SNE-ASTN-PP
ATTN: R. J. Richmond
Huntsville, Alabama 35812

Norman T. Musial
NASA, Lewis Research Center
21000 Brookpark Road
Cleveland, OH 44135

J. H. Rupe
Jet Propulsion Laboratory
California Institute of
Technology
48000 Oak Grove Drive
Pasadena, CA 91103

J. G. Thibadaux
NASA, Manned Spacecraft Center
Houston, TX 77058

Illinois Institute of Technology
Room 200 M.H.
ATTN: T. P. Torda
3300 S. Federal Street
Chicago, IL 60616

W. W. Wharton AMSMI-RKL
U.S. Army Missile Command
Redstone Arsenal, Alabama 35808

Lt. Col. Richard W. Haffner (NAE)
Air Force Office of Scientific
Research
1400 Wilson Boulevard
Arlington, VA 22209

Report Control Office
NASA, Lewis Research Center
21000 Brookpark Road
Cleveland, OH 44135